Nanoscale

COMMUNICATION

Facile Single-Step Synthesis of Ternary Multicore Magneto-Plasmonic Nanoparticles

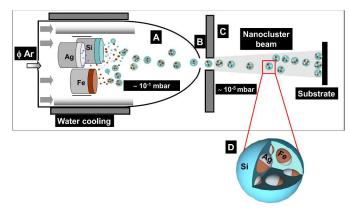Maria Benelmekki, Murtaza Bohra, Jeong-Hwan Kim, Rosa E.Diaz, Jerome Vernieres, Panagiotis Grammatikopoulos, Mukhles Sowwan*

We report a facile single-step synthesis of ternary hybrid nanoparticles (NPs) composed of multiple dumbbell-like Iron-Silver (FeAg) cores encapsulated by a silicon (Si) shell using a versatile co-sputter gas-condensation technique. In comparison to previously reported binary magneto-plasmonic NPs, the advantage conferred by a Si shell is to bind the multiple magneto-plasmonic (FeAg) cores together and prevent them from aggregation at the same time. Further, we demonstrate that the size of the NPs and number of cores in each NP can be modulated over a wide range by tuning the experimental parameters.

In recent years, progress in nanomaterials synthesis has made it possible to mix two or more different materials to obtain binary, ternary and multicomponent hybrid nanoparticles. Thus, different functionalities can be combined in one single nanoparticle, and enhanced properties can even be realized due to the coupling between the different components.[1-6] In particular, hybrid nanoparticles composed of a magnetic component and a noble metal are attractive because of their combined magnetic and plasmonic properties. However, to gain control over the size and morphology of the hybrid nanoparticles complicated multistep procedures that include nucleation and growth of a second and even a third phase on a single component seed nanoparticle are usually required.[1-10] Herein, we report a facile single-step synthesis of ternary biocompatible multicore magneto-plasmonic nanoparticles. The nanoparticles were produced by sputtering of high-purity Fe, Ag and Si targets simultaneously using a modified magnetron-sputter inert-gas condensation system as illustrated in Figure 1. Detailed experimental procedures and deposition conditions are provided in Electronic Supplementary Information (ESI).

Bright field transmission electron microscopy (BF TEM) micrographs (Figures 2a,b,c,d) reveal a distinctive structure of multiple cores encapsulated by an amorphous shell as demonstrated in (a) one core, (b) two cores, (c) three cores,

and (d) four cores, respectively. Panoramic TEM images showing the distribution of the multicore NPs are provided in ESI (Figure S6).
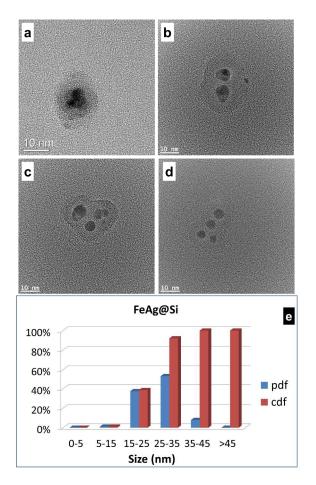

Fig. 1 Illustration of the modified magnetron sputter inert-gas condensation system used in this study, showing the three co-sputtered targets (A) the aggregation zone; (B) the differential pumping aperture; (C) the main chamber where particles are deposited on substrates. (D) Sketch of the obtained hybrid nanoparticles.

The size probability distribution function (pdf) (Figure 2e) calculated over 98 imaged nanoparticles shows that the size of a nanoparticle is proportional to the number of cores encapsulated by its Si shell, while the cumulative distribution function (cdf) shows that 40% of the nanoparticles have single or double cores with a size < 25nm and the remaining 60% have three or four cores with a size < 45nm. On the one hand, the Si shell binds the multiple FeAg cores together and, on the other hand, prevents them from aggregation. Scanning transmission electron microscopy (STEM) micrograph (Figure 3a) shows a contrast difference between the core domains, which are connected in a dumbbell-like shape. The Ag domain appears brighter than the Fe domain because the higher atomic number of Ag results in a greater detected signal relative to that of Fe.
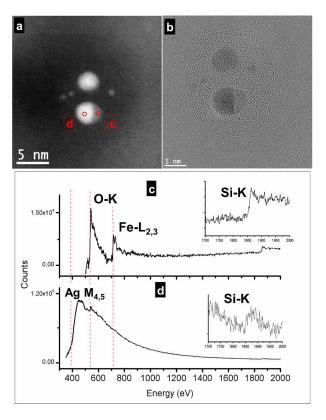
Fig. 2 Morphology of the nanoparticles. TEM micrographs showing nanoparticles with (a) one core, (b) two cores, (c) three cores and (d) four cores, respectively. The scale bar is 10 nm. (e) The size probability distribution function (pdf), and cumulative distribution function (cdf) calculated over 98 nanoparticles.

A HRTEM image of the same nanoparticle, with unchanged orientation with respect to the electron beam (Figure 3b) indicates that the Ag domains are crystalline while the Fe domains and the Si shell are amorphous. Energy electron loss spectroscopy (EELS) spectra taken at 2 points with different brightness contrast (Figures 3c and 3d) confirm the FeAg dumbbell-like core and Si shell structure. The size of the nanoparticles and the number of cores encapsulated in each nanoparticle can be modulated by controlling the deposition parameters as follow: 1) Adjusting the powers on each target, we control plasma density on the surface on each target and then we control the size and crystallinity of the formed clusters (more details are provided in section 7 of ESI). 2) Increasing the pressure in the aggregation zone (Figure 1 A), we increase the probability of multiples collisions between the different specimens. 3) Introducing Ar gas at the
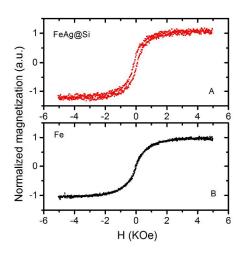
differential pumping aperture level (Figure 1 B), we increase the residence time of the NPs inside the aggregation zone enhancing the coalescence between the NPs (See ESI). On the other hand, because of the large positive free energy of Fe and Ag mixing, segregation of the elements forming core/shell or dumbbell-like structures is expected.[9,11] However, from our TEM study, an almost exclusive formation of dumbbell-like structure was observed. A plausible explanation of this behavior is that when Fe and Ag nanoparticles collide in the aggregation zone, their energy is not enough to induce their complete coalescence, so that only dumbbell-like structures are formed. Moreover, due to the low surface energy of amorphous silicon (1.05 J m^{-2}),[12] Si clusters cover the surface of FeAg nanoparticles, resulting in a core/shell structure. Finally, during their flight along through aggregation zone, FeAg/Si core/shell nanoparticles collide and partially coalesce with each other resulting in multicore and irregular-shaped NPs (FeAg@Si NPs).

Fig. 3 Microstructure and composition of the nanoparticles. (a) Z-contrast STEM and (b) BF HRTEM images of the same nanoparticle, with unchanged orientation with respect to the electron beam. (c) EELS spectra showing that the cores are composed of Fe and Ag domains in a dumbbell-like shape, and the shell is composed of Si.
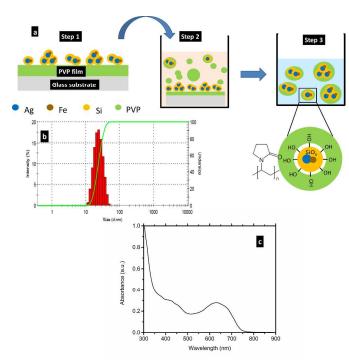
The normalized magnetization of the Fe-Ag@Si NPs at 300 K as a function of the applied magnetic field is depicted in Figure 4. A typical ferromagnetic behavior (red curve) is

observed with a coercivity of ~ 102 Oe in contrast to pure Fe NPs deposited under the same experimental conditions (without Ag or Si), which show nearly superparamagnetic behavior (black curve). The ferromagnetic behavior of the Fe-Ag@Si nanoparticles can be attributed to the modification of anisotropy at the Fe-Ag and Fe-Si interfaces. [13]

Fig. 4 Magnetization curves at 300 K of (A) FeAg@Si NPs and (B) Fe NPs prepared under the same experimental conditions. FeAg@Si NPs exhibit ferromagnetic behavior, while Fe nanoclusters show superparamagnetic behavior as expected.

X-ray photoelectron spectroscopy (XPS) measurements (supporting information) suggest that the oxidation state of Fe domains is dominated by the Fe^{3+} state and the amorphous Si shell is fully oxidized. To harvest the ternary nanoparticles in solution, the hybrid NPs were deposited on a glass substrate pre-coated with Polyvinylpyrrolidone (PVP) film. The harvesting procedure employed is straightforward and cost-effective. The PVP-NPs composite supported on glass was ultrasonicated in methanol for 15min, then dispersed in ultra-pure water as shown in Figure 5a. The size distribution and the stability of the colloidal suspension of nanoparticles were evaluated using dynamic light scattering and zeta potential measurements. The nanoparticles show a size distribution from 10-50 nm in agreement with the TEM results (Figure 5b) and a Zeta potential value of -30 mV. Both DLS and Zeta Potential data were acquired from twelve runs per measurement and showed a uniform distribution between runs, corresponding to a high quality criterion. The sample also retained its outstanding colloidal suspension stability in water (> 6 months).The optical properties of the hybrid nanoparticles were determined using UV-Vis absorption spectroscopy (Figure 5c). Fe-Ag@Si nanoparticles exhibit a strong red- shifted surface plasmon resonance peak centered at 620nm (compared to Ag nanoclusters prepared under the

same conditions, see supporting information). This red shift can be attributed to the plasmonic coupling at the interface between the Ag nanodomains and the surrounding oxidized Fe and Si.[14,15]

Fig 5. Stability and optical properties of the ternary hybrid NPs in solution. (a) Schematic of the exfoliation procedure developed in the present work. (Step 1) FeAg@Si NPs were deposited on a spin coated PVP (polyvinylpyrrolidone) film on glass substrate. (Step 2) FeAg@Si/PVP/glass samples were immersed in methanol and sonicated for 15 min, then separated to remove excess PVP. (Step 3) After washing precipitated FeAg@Si/PVP NPs with methanol, NPs were re-suspended in ultrapure water (b) Dynamic light scattering histogram showing the size distribution of the hybrid nanoparticles (c) UV-Vis optical absorption spectra of the dispersed nanoparticles solution.

In summary, multicomponent hybrid NPs composed of dumbbell like FeAg cores encapsulated by a Si shell have been fabricated using a versatile single-step co-sputter gas-condensation method. The fabricated ternary nanoparticles combine magnetic and plasmonic functionalities, with good colloidal suspension stability, which makes them attractive candidates for use in biomedical and nanotechnology contexts, from basic scientific research to commercially useful technologies. The utilized single-step co-sputtering technique in this study is general and can be applied to design and fabricate other exotic nanostructures as well.

Notes and references

Authors Affiliations: Nanoparticles by Design Unit, Okinawa Institute of Science and Technology (OIST) Graduate University. 1919-1 Tancha, Onna Son, Okinawa, 904-0495,Japan.

Corresponding Author: Mukhles@oist.jp

1 Wang, C. Xu, H. Zeng, S. Sun, *Adv. Mater*. 2009, **21**, 3045–3052;

2 I. Parsina, C. DiPaola, F. Baletto, *Nanoscale*, 2012, **4**, 1160-1166;

3 H. Yu, M. Chen, P. M. Rice, S. X. Wang, R. L. White, S. Sun *Nano Lett*. 2005, **5**, 379-382;

4 H. Gu, Z. Yang, J. Gao, C. K. Chang, B. Xu, *J. Am. Chem. Soc*. 2005, **127**, 34-35;

5 Y. Lu, H. Xiong, X. Jiang, Y. Xia, *J. Am. Chem. Soc*. 2003, **125**, 12724-12725;

6 X. Meng, H. C. Seton, L. T. Lu, I. A. Prior, N. T. K. Thanh, B. Song, *Nanoscale* 2011, **3**, 977-984.

7 H. Zeng, S. Sun, *Adv. Funct. Mater*. 2008, **18**, 391-400;

8 Perro, S. Reculusa, S. Ravaine, E. Bourgeat-Lami, E. Duguet J. Mater. Chem. 2005, **15**, 3745-3760;

9 Y.H. Xu, J.P. Wang, *Adv. Mater*. 2008, 20, 994-999;

10 V. Skumryev, S. Stoyanov, Y. Zhang, G. Hadjipanayis, D. Givord, J. Nogués *Nature* 2003, **423**, 850-853.

11 A. Elsukova, Z.A. Li, C. Möller, M. Spasova, M. Acet, M. Farle, M. Kawasaki, P. Ercius, T. Duden Phys. Status Solidi A 2011, 208, 2437-2442.

12 S. Hara, S. Izumi, T. kumagai, S. Sakai, Surface Science 2005, 585, 17-24.

13 J. Alonso, M.L. Fdez-Gubieda, G. Sarmiento, J. Chaboy, R. Boada, A.G. Prieto, D. Haskel, M.A. Laguna-Marco, J.C. Lang, C. Meneghini, L.F. Barquın, T. Neisius, I. Orue, *Nanotechnology* 2012, **23**, 025705.

14 A. Alqudami, S. Annapoorni, Plasmonics 2007, **2**, 5 ;Y. Zhai, L. Han, P. Wang, G. Li, W. Ren, L. Liu, E. Wang, S. Dong *ACS Nano 2011, 5, 8562-8570.*

15 N.I. Cade, T. Ritman-Meer, K.A. Kwakwa, D. Richards, *Nanotechnology* 2009, **20**, 285201.

Nanoscale Accepted Manuscript